NANO MICRO small

Supporting Information

for *Small,* DOI: 10.1002/smll.202206085

Understanding Humidity-Enhanced Adhesion of Geckos: Deep Neural Network-Assisted Multi-Scale Molecular Modeling

Tobias Materzok, Hossein Eslami, Stanislav N. Gorb, and Florian Müller-Plathe*

SUPPORTING INFORMATION

Understanding Humidity-enhanced Adhesion of Geckos: Deep Neural Network-assisted Multi-scale Molecular Modeling

Tobias Materzok Hossein Eslami Stanislav N. Gorb Florian Müller-Plathe*

Tobias Materzok, Prof. Dr. Hossein Eslami, Prof. Dr. Florian Müller-Plathe
Email Address: t.materzok@theo.chemie.tu-darmstadt.de
Eduard-Zintl-Institut für Anorganische und Physikalische Chemie and Profile Area Thermofluids and Interfaces
Technische Universität Darmstadt
Alarich-Weiss-Str. 8
D-64287 Darmstadt
Germany
Prof. Dr. Hossein Eslami
Department of Chemistry, Colleges of Sciences
Persian Gulf University
Boushehr 75168
Iran
Prof. Dr. Stanislav N. Gorb
Zoological Institute Functional Morphology and Biomechanics
Kiel University
Am Botanischen Garten 1-9
D-24118 Kiel
Germany

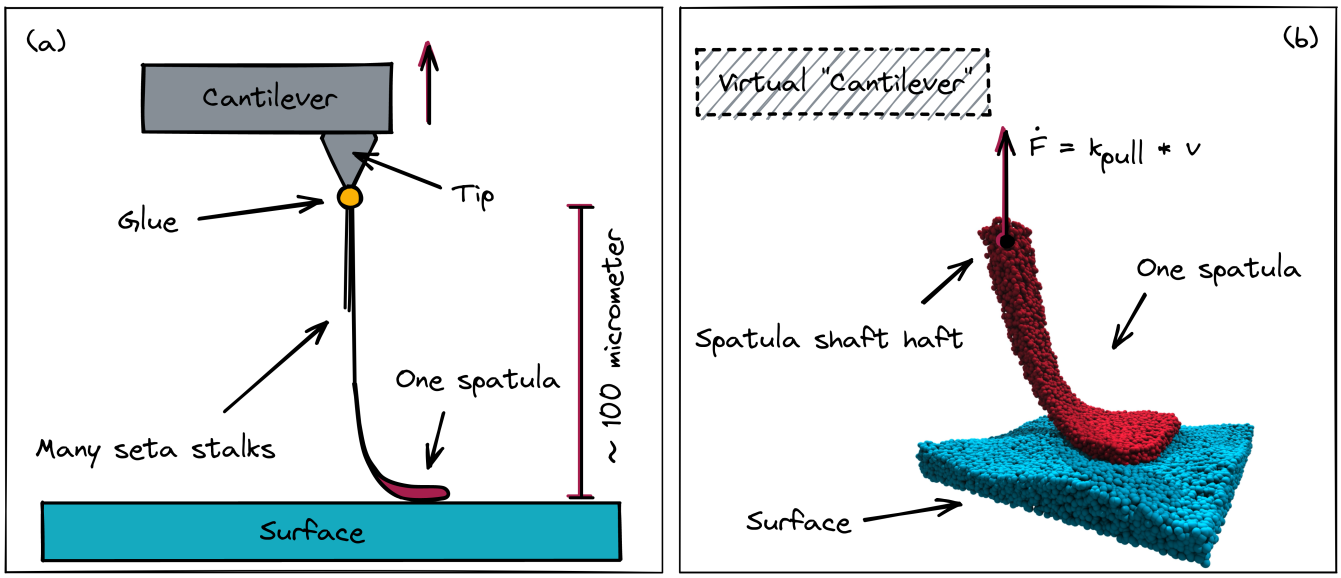

Figure S1: (A) Experimental setup of atomic force microscopy (AFM) experiments that investigate gecko single-spatula adhesion, e.g., by Huber et al.[1][2][3]. A single seta is glued to a cantilever, and then an ion beam is used to cut off everything except isolated single spatulae. Since setae are around 100 μm long, the surface is far away from the AFM tip. (B) The simulation setup used in this work and explained in more detail elsewhere[4]. A virtual "cantilever" (e.g., a non-interacting particle) is linked to the spatula shaft haft with a harmonic spring and pulled vertically upwards.

1 Deep neural network

A deep neural network is a network of nodes. A fully connected layer consists of N hidden layers, and each node of one hidden layer is connected to all nodes of the previous hidden layer, as well as with all nodes of the next hidden layer. Each node is essentially an activation function that computes the output using the sum of the node's inputs that are weighted by their corresponding weight w_{ij}. Linear activation functions like the Rectified Linear Unit (ReLU) or the Scaled Exponential Linear Unit[5] (SELU) are most commonly used for regression problems like ours. The output of one node o_j is the transform of the sum over all inputs $w_{1j} \cdot x_1$ to $w_{nj} \cdot x_n$, essentially $\sum_{i=1}^{n} w_{ij} x_i$ with the activation function ϕ. We use a bias b as well (Equation 1).

$$o_j = \phi(\sum_{i=1}^{n} w_{ij} x_i + b) \tag{1}$$

where

$$\phi(x) = \begin{cases} x, & \text{if } x > 0. \\ \alpha e^x - \alpha, & \text{if } x \leq 0. \end{cases} \tag{2}$$

The networks' weights are tuned such that the input to the network reproduces the output. The back-propagation algorithm computes the gradient of a loss function with respect to the weights that can then be used to update weights to minimize the loss using, e.g., gradient descent. Grid-based hyperparameter search found optimal results for network architecture, activation functions of layers, loss function and optimization method. It resulted in us using the mean squared error as the loss function and Adam[6] for stochastic optimization. In this work, we use the Keras library[7] on top of Tensorflow[8].

Figure 2 illustrates the DNN network architecture. The input vector is connected to a fully connected layer (6x64). We use a Keras Gaussian noise layer with a standard deviation of 0.1 to regularize the inputs (the input ranges from 1 to 3000 kJ mol^{-1} nm^{-2}). To reduce overfitting and improve model generalization, we applied a Keras Gaussian noise layer to the output. The standard deviation of the latter Gaussian is

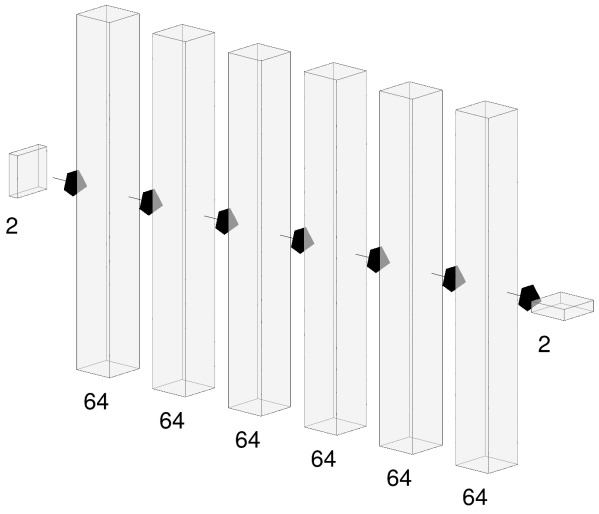

Figure S2: Structure of the deep neural network with two inputs k and k_b and two outputs E and ν.

wt%	RH (%)	E_{meso} (GPa)	v_{meso}	k (kJ mol^{-1} nm^{-2})	k_b (kJ mol^{-1} nm^{-2})
0	0	4.529 ± 0.033	0.409 ± 0.002	198	1282
5	52	4.038 ± 0.045	0.435 ± 0.002	109	1250
10	86	3.838 ± 0.040	0.422 ± 0.002	135	1139
20	100	2.247 ± 0.025	0.496 ± 0.004	3	794

Table S1: The predicted anisotropic force constant coefficients of the mesoscale keratin material and the corresponding Young' moduli and Poisson' ratios.

computed as 10% of the standard deviation of the mean over the whole output data, where the previously computed Young' moduli E and Poisson' ratios ν are used as the output.

We should note here that we scaled the Poisson ratio to be in the same order of magnitude as Young's modulus. Since E of our united-atom gecko keratin ranges from around 2000 MPa to 4500 MPa and Poisson's ratio from 0.4 to 0.5, we multiplied the latter by 10000 to make ν range between 4000 and 5000. Generally, it makes training a neural network easier if all input and outputs are regularized to the same scale.

Except for the output layer, which uses a linear activation function $\phi(x) = x$, all layers use the scaled exponential linear unit[5] (SELU) activation function (Equation 2) with a LeCun[9] kernel initializer and biases are initialized with ones.

2 Computational Details

The united-atom (UA) gecko keratin model uses the GROMOS 54A7 force field[10, 11, 12, 13] for all atoms present in the system, keratin protein and surface.

In an earlier coarse-grained study[14], we found that only the gecko keratin's intrinsically disordered protein regions (IDRs) directly contact the surface and not the beta-folded region of the keratin protein that polymerizes into nanofibrils. Thus, only the IDRs of the gecko keratin protein are responsible for the adhesive energetic interaction between spatula and surface. Therefore, we amorphized a gecko beta-keratin protein (Ge-cprp-9) and only considered the intrinsically disordered parts of the protein.

The exact equilibration protocol, including energy minimization, amorphization at 1300 K with a subsequent cooldown, and multi-step equilibrations in the NPT ensemble with and without soft-core potentials, go beyond this SI.

United-atom keratin simulations are carried out using the GROMACS 2018 software package[15], the GROMOS 54A7 force field[10, 11, 12, 13], and the SPC/E water model[16]. The production runs to calculate Young's modulus are performed in three-dimensional periodic boundary conditions (PBC). The

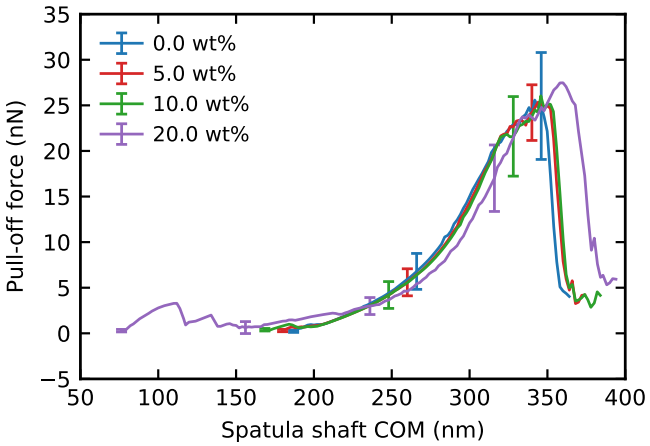

Figure S3: Average force-displacement curves of the mesoscale spatula pull-off at 4 different implicit water contents (legend). The loading rate is $1.66 \cdot 10^{12}$ pN s^{-1}. The average force curve is computed from 10 independent samples, and the standard deviation of the mean is used as the error.

timestep is 2 fs, and a velocity rescale[17] thermostat keeps the temperature at 300 K. A semi-isotropic Berendsen[18] barostat with a compressibility of $4.5 \cdot 10^{-5}$ bar^{-1} in x and y, and a compressibility of 0 bar^{-1} in z, keeps the pressure of the system at 1 bar. Therefore, only size fluctuations in x and y are possible. The system is uniformly strained in the z dimension with a straining rate of 0.00001 nm ps^{-1} = 1.0 mm s^{-1}. Production runs are repeated five times for five independently generated systems ($n = 25$). Young's modulus is computed with a linear fit to the first 1% strain. Poisson's ratio is the average over strain 1% to 5% and calculated using equilibrium runs, i.e., straining the system and running production run at a constant strain.

Mesoscale keratin simulations use the GROMACS 2018 and 2021 software package[15] and are carried out with the force field we derived previously[4], except for the bond force field parameterized in this work using the DNN. The timestep is 20 fs. Van der Waals interactions are modeled using a Lennard-Jones (12-6) potential with a cutoff of 12 nm and the potential-shift-Verlet scheme[19] as a cutoff modifier for a physically[20] smooth transition at the cutoff. A velocity rescale[17] thermostat with a coupling time of $\tau_T = 2$ ps keeps the temperature at 300 K. For simulations in the NPT ensemble used for validating Young's modulus and Poisson's ratio of the DNN predicted anisotropic force constant coefficients k and k_b a Berendsen[18] semi-isotropic barostat is used, as explained above and in more detail in previous work[4].

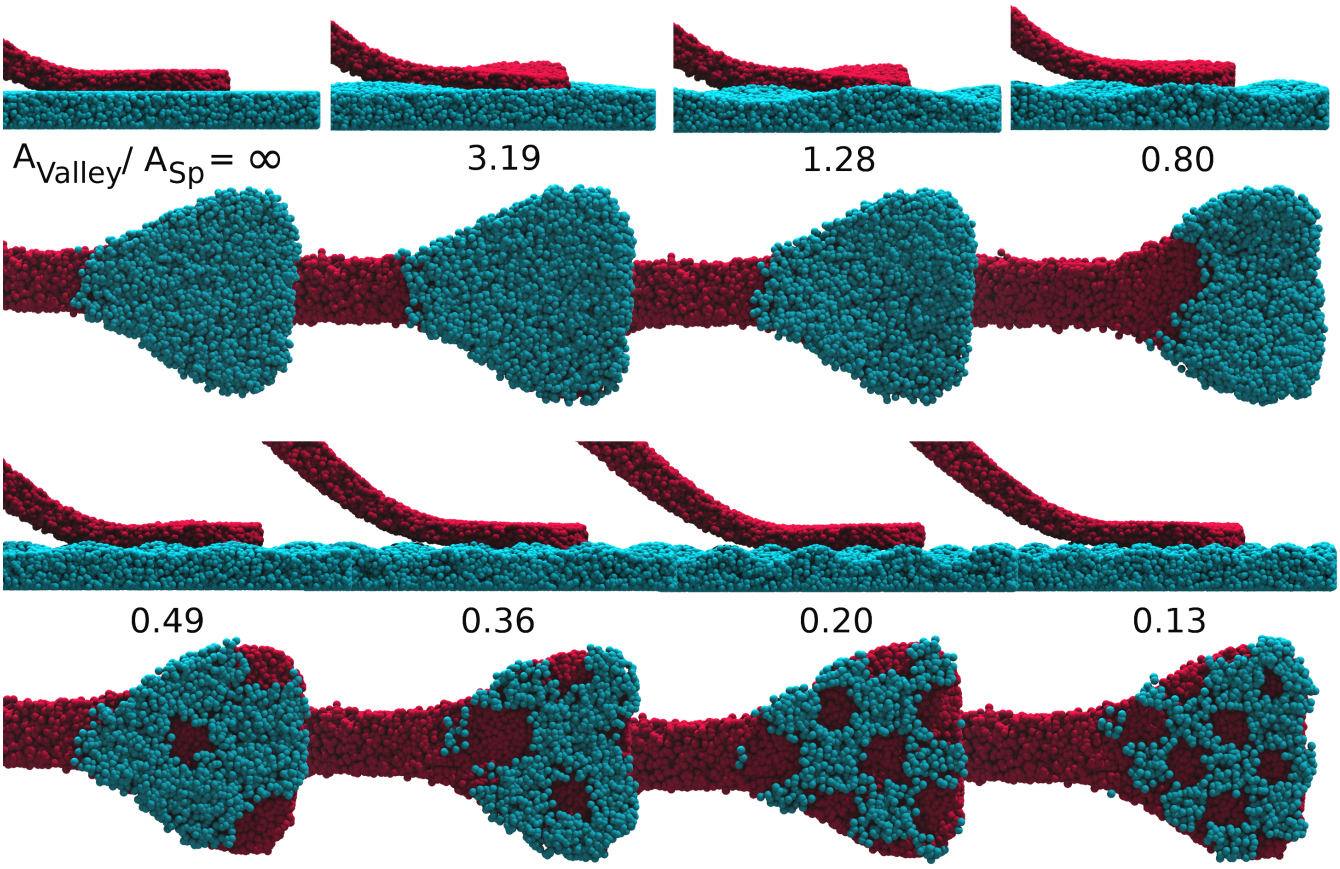

Figure S4: (Top) Spatulae at a material softness corresponding to a low ($\approx 0\%$) humidity (0% water content) attached to rough surfaces of increasing peak density (from top left with $\rho_{\mathrm{Peak}} = 0\ \mu\mathrm{m}^{-2}$ to bottom right with 394.12 $\mu\mathrm{m}^{-2}$). The average height between the peak and valley is 16 nm for all surfaces. (Bottom) View from below the surface, where only surface beads (cyan) that interact with the spatula (red) are shown. The ratio $A_{\mathrm{valley}}/A_{\mathrm{Sp}}$ between the area between peaks and the spatula area is noted underneath each surface.

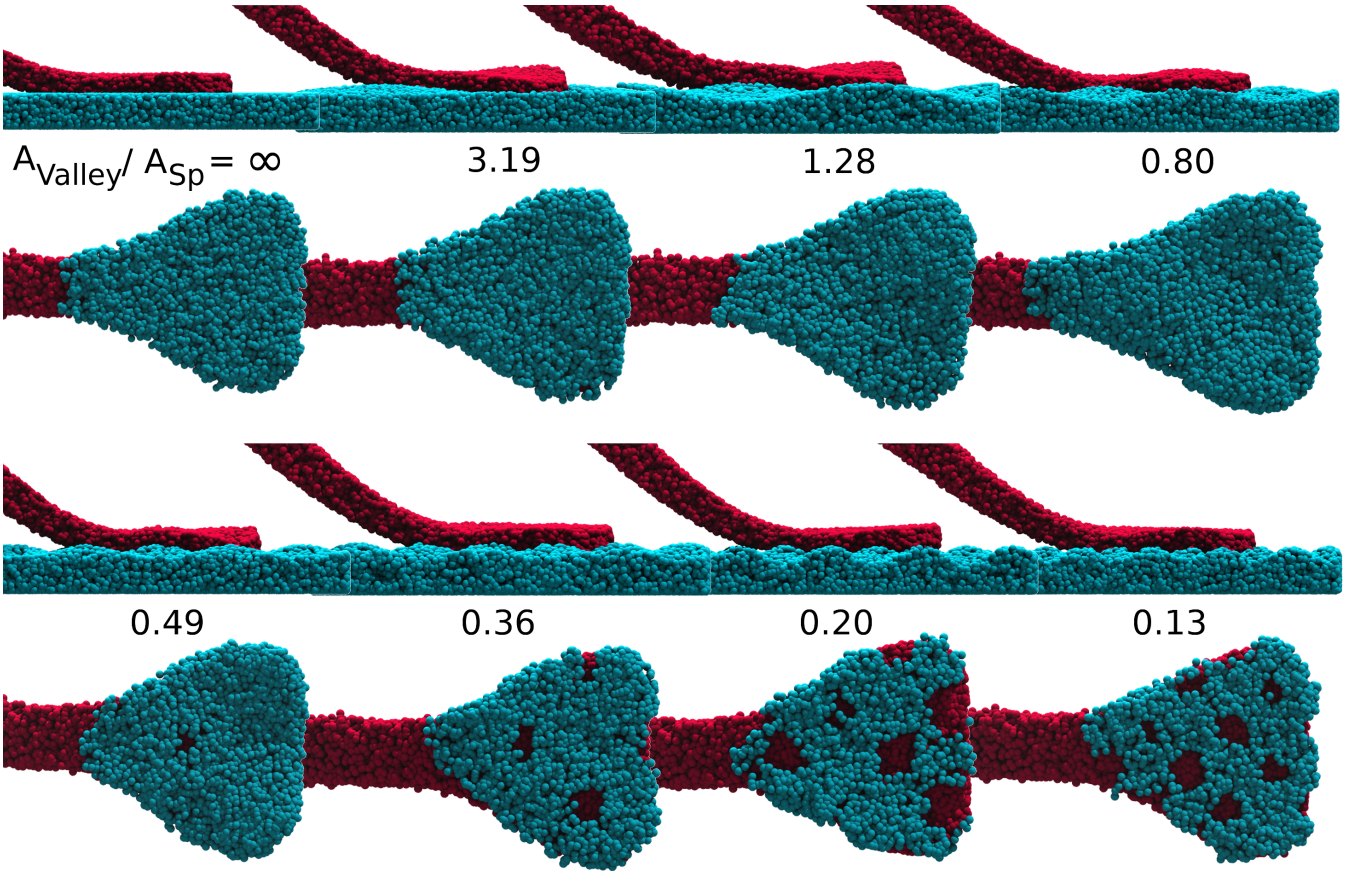

Figure S5: (Top) Spatulae at a material softness corresponding to a high (> 86%) humidity (20% water content) attached to rough surfaces of increasing peak density (from top left with $\rho_{\mathrm{Peak}} = 0\ \mu\mathrm{m}^{-2}$ to bottom right with 394.12 $\mu\mathrm{m}^{-2}$). The average height between the peak and valley is 16 nm for all surfaces. (Bottom) View from below the surface, where only surface beads (cyan) that interact with the spatula (red) are shown. The ratio $A_{\mathrm{valley}}/A_{\mathrm{Sp}}$ between the area between peaks and the spatula area is noted underneath each surface.

References

[1] G. Huber, H. Mantz, R. Spolenak, K. Mecke, K. Jacobs, S. N. Gorb, E. Arzt, *Proc. Natl. Acad. Sci. U.S.A.* **2005**, *102*, 45 16293.

[2] G. Huber, S. N. Gorb, N. Hosoda, R. Spolenak, E. Arzt, *Acta Biomater.* **2007**, *3*, 4 607.

[3] G. Huber, S. N. Gorb, R. Spolenak, E. Arzt, *Biol. Lett.* **2005**, *1*, 1 2.

[4] T. Materzok, D. De Boer, S. N. Gorb, F. Müller-Plathe, *Small* **2022**, *18*, 35 2201674.

[5] G. Klambauer, T. Unterthiner, A. Mayr, S. Hochreiter, *arXiv:1706.02515 [cs, stat]* **2017**, arXiv: 1706.02515.

[6] D. P. Kingma, J. Ba, *arXiv:1412.6980 [cs]* **2017**, arXiv: 1412.6980.

[7] F. Chollet, Keras, **2015**, URL `https://keras.io`.

[8] Martín Abadi, Ashish Agarwal, Paul Barham, Eugene Brevdo, Zhifeng Chen, Craig Citro, Greg S. Corrado, Andy Davis, Jeffrey Dean, Matthieu Devin, Sanjay Ghemawat, Ian Goodfellow, Andrew Harp, Geoffrey Irving, Michael Isard, Y. Jia, Rafal Jozefowicz, Lukasz Kaiser, Manjunath Kudlur, Josh Levenberg, Dandelion Mané, Rajat Monga, Sherry Moore, Derek Murray, Chris Olah, Mike Schuster, Jonathon Shlens, Benoit Steiner, Ilya Sutskever, Kunal Talwar, Paul Tucker, Vincent Vanhoucke, Vijay Vasudevan, Fernanda Viégas, Oriol Vinyals, Pete Warden, Martin Wattenberg, Martin Wicke, Yuan Yu, Xiaoqiang Zheng, TensorFlow: Large-Scale Machine Learning on Heterogeneous Systems, **2015**, URL `https://www.tensorflow.org/`.

[9] Y. Lecun, L. Bottou, Y. Bengio, P. Haffner, *Proc. IEEE* **1998**, *86*, 11 2278.

[10] L. D. Schuler, X. Daura, W. F. v. Gunsteren, *J. Comput. Chem.* **2001**, *22*, 11 1205.

[11] C. Oostenbrink, A. Villa, A. E. Mark, W. F. V. Gunsteren, *J. Comput. Chem.* **2004**, *25*, 13 1656.

[12] N. Schmid, A. P. Eichenberger, A. Choutko, S. Riniker, M. Winger, A. E. Mark, W. F. van Gunsteren, *Eur. Biophys. J.* **2011**, *40*, 7 843.

[13] W. Huang, Z. Lin, W. F. van Gunsteren, *J. Chem. Theory Comput.* **2011**, *7*, 5 1237.

[14] T. Materzok, S. N. Gorb, F. Müller-Plathe, *Soft Matter* **2022**, *18*, 6 1247.

[15] B. Hess, C. Kutzner, D. van der Spoel, E. Lindahl, *J. Chem. Theory Comput.* **2008**, *4*, 3 435.

[16] H. J. C. Berendsen, J. R. Grigera, T. P. Straatsma, *J. Phys. Chem.* **1987**, *91*, 24 6269.

[17] G. Bussi, D. Donadio, M. Parrinello, *J. Chem. Phys.* **2007**, *126*, 1 014101.

[18] H. J. C. Berendsen, J. P. M. Postma, W. F. van Gunsteren, A. DiNola, J. R. Haak, *J. Chem. Phys.* **1984**, *81*, 8 3684.

[19] S. Páll, B. Hess, *Comput. Phys. Commun.* **2013**, *184*, 12 2641.

[20] D. van der Spoel, P. J. van Maaren, *J. Chem. Theory Comput.* **2006**, *2*, 1 1.

Table of Contents

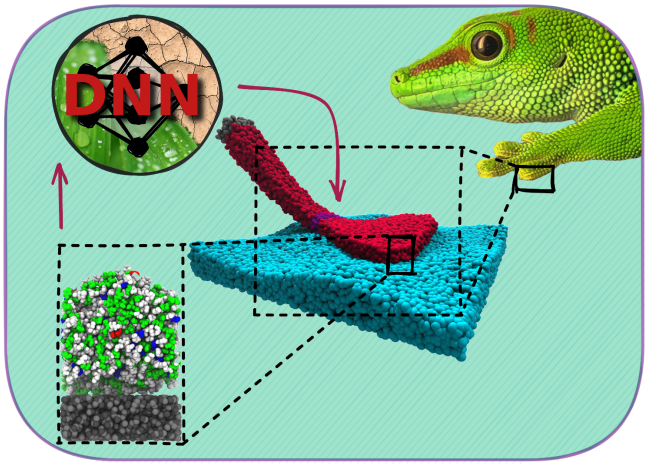

The prominent material-softening hypothesis in humidity-enhanced gecko adhesion is investigated by a bottom-up coarse-grained mesoscale model of an entire gecko spatula designed without explicit water particles present, so that capillary action and water-mediation are excluded. We show that on nanoscopic flat surfaces, the softening of keratin by water uptake cannot nearly account for the experimentally observed increase in gecko sticking power.